Angiotensin II infusion into ApoE$^{-/-}$ mice: a model for aortic dissection rather than abdominal aortic aneurysm?

Running title: **Ang II infusion into ApoE $^{-/-}$ mice**

Bram Trachet, PhD[1,2], Lydia Aslanidou[2], Alessandra Piersigilli, PhD[3], Rodrigo A. Fraga-Silva, PhD[2] , Jessica Sordet-Dessimoz, PhD[4], Pablo Villanueva-Perez, PhD [5], Marco F.M. Stampanoni, PhD [5,6], Nikolaos Stergiopulos, PhD [2], Patrick Segers, PhD [1]

[1] IBiTech - bioMMeda, Ghent University-iMinds Medical IT, Ghent, Belgium

[2] Institute of Bioengineering, Ecole Polytechnique Fédérale de Lausanne, Lausanne, Switzerland

[3] Weill Medicine Cornell New York, NY, United States

[4] Histology Core Facility, Ecole Polytechnique Fédérale de Lausanne, Lausanne, Switzerland

[5] Swiss Light Source, Paul Scherrer Institut, Villigen, Switzerland

[6] Institute for Biomedical Engineering, University and ETH Zürich, Zürich, Switzerland

Manuscript: 9166 words, 7 Figures

Bram Trachet

LHTC STI IBI EPFL
BM 5128 Station 17
CH-1015 Lausanne (Switzerland)
Tel: +41 21 693 83 81
bram.trachet@epfl.ch

Angiotensin II infusion into ApoE$^{-/-}$ mice: a model for aortic dissection rather than abdominal aortic aneurysm?

Bram Trachet, Lydia Aslanidou, Alessandra Piersigilli, Rodrigo A. Fraga-Silva, Jessica Sordet-Dessimoz, Pablo Villanueva-Perez, Marco F.M. Stampanoni, Nikolaos Stergiopulos, Patrick Segers.

Cardiovascular Research 2017, 113, 1230-1242

doi:10.1093/cvr/cvx128

Abstract

Aims: Angiotensin II-infused ApoE $^{-/-}$ mice are a popular mouse model for preclinical aneurysm research. Here, we provide insight in the often-reported but seldom-explained variability in shape of dissecting aneurysms in these mice.

Methods and Results: N=45 excised aortas were scanned ex vivo with phase-contrast X-ray tomographic microscopy. Micro-ruptures were detected near the ostium of celiac and mesenteric arteries in 8/11 mice that were sacrificed after 3 days of angiotensin II-infusion. At later time points (after 10, 18 and 28 days) the variability in shape of thoraco-abdominal lesions (occurring in 31/34 mice) was classified based on the presence or absence of a medial tear (31/31), an intramural hematoma (23/31) or a false channel (11/23). Medial tears were detected both in the thoracic and the abdominal aorta and were most prevalent at the left and ventral aspects of celiac and mesenteric arteries. The axial length of the hematoma strongly correlated to the total number of ruptured branch ostia (r^2=0.78) and in 22/23 mice with a hematoma the ostium of the left suprarenal artery had ruptured. Supraceliac diameters at baseline were significantly lower for mice that did not develop an intramural hematoma, and the formation of a false channel within that intramural hematoma depended on the location, rather than the length, of the medial tear.

Conclusions: Based on our observations we propose an elaborate hypothesis that explains how aortic side branches (i) affect the initiation and propagation of medial tears and the subsequent adventitial dissection and (ii) affect the variability in shape of dissecting aneurysms. This hypothesis was partially validated through the live visualization of a dissecting aneurysm that formed during micro-CT imaging, and led us to the conclusion that angiotensin II-infused mice are more clinically relevant for the study of aortic dissections than for the study of abdominal aortic aneurysms.

Abbreviations

AAA: abdominal aortic aneurysm

PCXTM: Phase-contrast X-ray Tomographic Microscopy

AD: Aortic Dissection

Ang II: Angiotensin II

Micro-CT: micro-computed tomography

IMH: Intramural hematoma

Throughout the manuscript, a consistent terminology has been used to avoid confusion between different types of lesions that were observed in the aortic wall. This terminology is explained in the online data supplement.

Introduction

In the last 15 years, Angiotensin II (Ang II) infusion into hypercholesterolaemic ApoE$^{-/-}$ mice has been a popular experimental model to study abdominal aortic aneurysm (AAA) [1-4]. Despite reproducing several clinical features of human AAA such as elastin degradation, macrophage infiltration, thrombus formation and re-endothelialization, other observations have remained unexplained, such as the suprarenal location, the role of aortic side branches and the strong heterogeneity in shape [5-8]. We recently used a novel synchrotron-based imaging technique (phase contrast X-ray tomographic microscopy; PCXTM) to show that the luminal dilatation in Ang II-infused, anti-TGF-beta injected C57Bl6 mice is the result of a medial tear, occurring near the ostium of suprarenal side branches. This tear was sometimes accompanied by a false channel with varying degrees of severity, and in some cases it resulted in the formation of an intramural (not intraluminal) hematoma (IMH) [9]. Differently from human aortic dissection (AD), the medial tear transected all of the elastic laminae and no re-entry into the true lumen was observed. We therefore described these lesions as dissecting AAAs, a term previously coined by other researchers[6,10]. In a follow-up review article we showed that our findings on dissecting aneurysms were compatible with virtually all existing (2D-imaging based) literature on the abdominal lesions of Ang II-infused ApoE $^{-/-}$ mice, and that the luminal dilatation in these models (if present at all) was more reminiscent of AD than of AAA[11, 12]. But while these observations provided new insights into the model, a number of intriguing research questions have remained unsolved, particularly regarding the mechanisms leading to the observed lesion variability. Here, we aimed to formulate answers and provide hypotheses on three issues that have dominated the debate on dissecting aneurysm formation during the past decades:

(i) **Location.** Why do dissecting aneurysms primarily develop near suprarenal side branches, and are some branches more affected than others [7]? A better understanding of the interaction between side branches and medial tears in Ang II-infused mice could lead to improve our understanding of the mechanisms leading to the formation of AAA and AD in humans [13].

(ii) **Variability.** Why do some animals develop a parallel false channel while others do not, and why do some animals die of transmural aortic rupture while others do not [11, 14]? A profound understanding of the formation and remodeling of the false channel in dissecting aneurysms in Ang II-infused mice could provide answers to the clinical question why AD patients with a partial thrombosis of the false lumen have a significantly worse prognosis than (i) patients without thrombosis and (ii) patients whose false lumen is completely occluded [15].

(iii) **Sequence of events.** Do minor side branches rupture independently, thus leading to the formation of both IMH and adventitial dissection, or does the adventitial dissection occur first, and are the ruptured side branches and IMH the consequence rather than the cause? And what is the role of the medial tear in this? A profound understanding of the sequence of events in the pathogenesis of dissecting aneurysms might provide us with some clues in the ongoing debate whether human IMH is the result of an AD or not [16].

In order to investigate these questions we present an observational, longitudinal study in which the thoraco-abdominal aorta of Ang II-infused ApoE$^{-/-}$ mice was followed up extensively in vivo with high-frequency ultrasound and contrast-enhanced micro-CT, and ex vivo with PCXTM and PCXTM-guided histology. The result is a unique database that has allowed for a detailed description of the mechanisms driving dissecting aneurysm formation.

Methods

A detailed description of the methodology is provided in the online data supplement.

Animal model. All the procedures were approved by the Ethical Committee of Canton Vaud, Switzerland (EC 2647.2) and performed according to the guidelines from Directive 2010/63/EU of the European Parliament on the protection of animals used for scientific purposes. Male ApoE $^{-/-}$ mice on a C57Bl/6 background were purchased from Janvier (Saint Berthevin, France). At the age of 12 weeks, n=47 mice (body weight: 28.0 ± 2.2 g) were implanted with a 200 µl osmotic pump (model Alzet 2004; Durect Corp, Cupertino, CA), filled with a solution of angiotensin II in saline 0.9% (Bachem, Bubendorf, Switzerland) as previously described [17]. Each pump infused Angiotensin II at 1000 ng/kg/min [18]. Prior to implantation the animals received buprenorphine (0.08 mg/Kg, subcutaneous) as analgesic and during pump implantation they were anesthetized with 1.5% isoflurane.

Sample sizes at different time points. Initially, n=12 angiotensin II–infused animals were included in the short-term in vivo imaging part of the study. N=1/12 animal of this group died with hemothorax after in vivo imaging at day 3 but prior to sacrifice. Since this animal had already developed a dissecting aneurysm it was moved to the long term imaging study. Another animal from the short-term study experienced a medial tear and IMH formation in the abdominal aorta during the micro-CT scan at day 3. This animal was treated as a special case of the short term study (see Figure 1). The remaining n=10 animals from the short term study were sacrificed at day 3 and studied for the occurrence of micro-ruptures. N=36 animals were included into the long-term study: n=35 from the initial study design and n=1 that was transferred from the short-term study. Of these, n=14 angiotensin II-infused animals died with hemothorax (n=8) or hemoabdomen (n=6). There was no significant difference in body weight between animals that died of transmural aortic rupture (28.4 ± 2.0 g) and animals that survived until sacrifice (28.0 ± 2.3 g). N=12/14 of these mice died at an early time point (i.e. prior to day 10), 1/14 died at day 14 and was thus included for in vivo imaging at day 10, and 1/14 died from aortic rupture after in vivo imaging at day 28 and was thus included in all in vivo imaging time points. The remaining 22 angiotensin II-infused animals were sacrificed after 10 (n=4), 18 (n=5) and 28 (n=13) days of angiotensin II infusion. In total n=45 abdominal aortic samples (n=11 samples from sacrificed animals in the short term-study, n=22 samples from sacrificed animals in the long term study and n=12/14 samples from animals that succumbed to hemothorax or hemoabdomen) were imaged with PCXTM.

In vivo ultrasound and micro-CT imaging. Animals were anesthetized with 1.5% isoflurane during the in vivo scans. Ultrasound imaging was performed with a high-frequency ultrasound device (Vevo 2100, VisualSonics, Toronto, Canada) using a linear array probe (MS 550D, frequency 22-55 MHz). Animals that were followed up in vivo with micro-CT were injected in the lateral tail vein with 4 µl/gram body weight of ExiTron nano 12000 (Miltenyi Biotec, Bergisch Gladbach, Germany) as previously described[9]. After the experiments, mice were anesthetized with Ketamine/Xylazine (100 mg/kg and 15 mg/kg, respectively) and the sacrifice was resolved following tissue collection.

Ex vivo PCXTM imaging. After sacrifice, the abdominal aorta was carefully excised and samples were fixed by immersion in freshly prepared 4% paraformaldehyde (PFA) at 4°C temperature for 24 hours. The samples were scanned at the TOMCAT beamline of the Swiss Light Source, Paul Scherrer Institut, Villigen, Switzerland as previously described [9].

PCXTM-guided histology. After PCXTM scanning, the samples were processed and embedded in paraffin according to standard histological procedures. Selected slides were stained with Haematoxylin-Eosin (H&E) to assess general morphology. Miller stain and Sirius red F3B (CI35782, Direct red 80) were combined to specifically highlight elastic fibers and collagen on the same section.

Ultrasound Image processing. Ultrasound Pulsed Doppler and M-Mode waveforms were traced within a custom-made environment platform in Matlab (Mathworks, Natick, MA) as previously described [14]. The circumferential cyclic Green-Lagrange strain (eq. 1) was calculated as an approximation for aortic compliance under the assumption of uniform strain around the vessel and unloaded configuration at minimal diameter.

$$Circ.strain = \frac{1}{2}\left[\left(\frac{D_{sys}}{D_{dia}}\right)^2 - 1\right] * 100\% \qquad \text{(eq. 1)}$$

Micro-CT and PCXTM image processing. All reconstructed 3D datasets were semi-automatically segmented into 3D models using the commercial software package Mimics (Materialise, Leuven, Belgium). We quantified the 3D volume of Exitron that infiltrated into the wall (as a proxy for the amount of damage to the wall), the number of side branches affected by Exitron infiltration, the number of branches in which the ostium was ruptured or a medial tear was observed, the axial length and volume of the intramural hematoma, the axial length of each medial tear, the volume of free-flowing blood outside the extrapolated walls of the tunica media and the circumferential and axial distribution of the medial tears with respect to the branches.

Histology image processing. All slides were photographed using an automated slide scanner (VI20-L100, Olympus) and analyzed using a dedicated plug-in in the open source software Fiji [19]. Combined thickness of the tunica intima and media as well as thickness of the tunica adventitia were measured on combined SR-Miller stains and a semi-quantitative measurement of both collagen deposition (on SR-Miller stains) and erythrocyte accumulation (on H&E stains) was performed.

Statistics. For the in vivo ultrasound measurements the baseline scans (i.e. scans that were obtained prior to pump implantation in the same animals) served as control data. For ex vivo PCXTM measurements we focused on the differences among lesions within the diseased population and therefore no control animals were used. For histology the control slides were obtained from the abdominal samples of saline-infused ApoE$^{-/-}$ mice that also served as controls in our previous study on ascending aortic aneurysm [20].

For all in vivo and ex vivo measurements incidence was defined as n1/n2, with n1 the number of mice in which a non-zero value was measured and n2 the total number of mice that was measured. The difference of incidence values in between time points or in between aortic locations was calculated using a chi-square test and pairwise comparisons of incidences were performed using a Tukey`s HSD multiple

comparisons test. The conditions for parametric testing were met for all ultrasound-based measurements and therefore their variation in between time points was calculated using a one-way Anova analysis. Post-hoc pairwise comparisons were performed using a Bonferroni correction and the independent comparisons between two different groups were calculated using a two-sided t-test. Since only a limited number of animals was sacrificed at each time point, most ex vivo experiments (PCXTM-based results and histology) had too few samples per time point to ascertain normality. These measurements were analyzed using a Kruskal-Wallis analysis, followed by a post-hoc Dunn`s test for pairwise comparisons and comparisons between two different groups were calculated using a wilcoxon test. In all analyses a p-value < 0.05 was considered significant (l), and a p-value < 0.001 was considered highly significant (ll).

Results

PCXTM-based analysis of lesions at the earliest time point

In 8/11 animals sacrificed after 3 days of Ang II infusion, the contrast agent Exitron that had been injected prior to in vivo micro-CT allowed us to detect micro-ruptures in the tunica media on the ex vivo PCXTM images [9, 20] (Figure 1a). These micro-ruptures occurred predominantly at the orifice of side branches, with the highest incidence occurring in the vicinity of the celiac and mesenteric arteries (Figure 1b). At the orifice of these two major branches, Exitron infiltration was most outspoken ventrally and sometimes occurred left or right of the ostium, but was never found on the dorsal aspect of the aorta (Figure 1c). In minor side branches (excluding the major branches mentioned in panel b), Exitron infiltration was found most often on dorsal branches, which were also the most abundant (Figure 1d). In one animal we serendipitously visualized the different phases of IMH formation during in vivo imaging (Figure 1e-i). A large volume of free-flowing blood was visible on the initial micro-CT scan (Figure 1e), while a follow-up micro-CT scan showed how 2.5 hours later most of the blood had already coagulated (Figure 1f, 1i). The animal was sacrificed 4 hours after the first micro-CT (Figure 1h), and ex vivo PCXTM images (Figure 1g) as well as image-guided histology (Figure 1i, bottom) revealed that a medial tear had been the source of free-flowing blood. In the time span of only a few hours, the adventitial dissection and IMH had extended far cranial and caudal of the medial tear.

PCXTM-based analysis of lesion variability in dissecting aneurysms

In animals that were found dead or that were sacrificed after 10, 18 and 28 days of Ang II-infusion and whose aorta was scanned with PCXTM (n=34), we identified three objective criteria to quantify the variability in dissecting aneurysm morphology. Different combinations of these criteria led to the description of seven distinct dissecting aneurysm morphologies, each with their respective incidence and mortality rates (Figure 2a). A first criterion was the presence (n=31/34) or absence (n=3/34) of at least one tear in the tunica media of the descending, thoracic or abdominal aorta. The 3 animals in which no thoraco-abdominal medial tear was found had died of ascending aortic aneurysm rupture at an early stage of Ang II infusion (Figure 2a). There was a significantly higher prevalence ($p<0.05$) of abdominal tears (i.e. caudal to the diaphragm, n=24/31) over descending and thoracic tears (i.e. cranial to the diaphragm, n=6/31). One animal presented medial tears in both the thoracic and the abdominal aorta (Figure 2b). A second criterion for lesion variability was the presence (n=23/31) or absence (n=8/31) of an IMH around the medial tear. All animals with an IMH also had a medial tear, but in animals without IMH the medial tear was simply covered by the adventitia. The IMH was characterized by a dissected adventitia and an intramural space filled with coagulated blood (Figure 2a). The length of the IMH was strongly correlated to the number of side branches in which the ostium was ruptured ($r^2=0.78$, Figure 2c), and mice with a thoracic medial tear had a significantly larger IMH than mice with an abdominal medial tear ($p<0.05$, Figure not shown). The abdominal volume of the IMH was significantly larger on the left and supraceliac aspects of the aorta than on the right and infraceliac aspects ($p<0.001$, Figure 2d).The third criterion to characterize lesion variability was the presence (n=11/31) or

absence (n=20/31) of a false channel (Figure 2a). All animals with a parallel false channel also had an IMH, but not all animals with an IMH had a false channel. The false channel was characterized by free-flowing blood that extended beyond the axial length of the medial tear from which it originated, thus forming a channel that ran in parallel to the true lumen. In animals with IMH but without false channel, the medial tear resulted in a local dilatation that remained at the level of the tear (Figure 2a). The length of the IMH was not different between animals with and animals without false channel ($p>0.1$, Figure not shown). Mortality due to rupture of the dissecting aneurysm was higher in animals with a thoracic tear, in animals with an IMH and in animals with a false channel, but none of these reached significance (Figure 2b).

PCXTM-based analysis of the relation between side branches, medial tears and adventitial dissections.

In animals that were sacrificed after 10, 18 or 28 days of Ang II-infusion, the highest amounts of Exitron were detected near the ostium of side branches (Figure 3a). The ostium of minor branches in the thoracic aorta was significantly less often infiltrated by Exitron than that of minor abdominal branches ($p<0.05$, Figure 3b) and the ostium of the celiac artery was significantly more often affected than the other major abdominal branches ($p<0.05$, Figure 3b). Medial tears occurred only very seldom near minor branches of the thoracic or abdominal aorta (8 tears on a total of +400 minor branches that was counted across all investigated mice, Figure 3c). Similar to the Exitron infiltration that was observed at the earliest time point (Figure 1b), medial tears in the abdominal aorta were significantly more frequent near the celiac artery and the mesenteric artery than near any of the other major branches ($p<0.05$, Figure 3c). The relation between the number of ruptured branch ostia and IMH length (Figure 2c) was not distributed evenly along the thoraco-abdominal aorta. Supraceliac minor branch ostia were ruptured significantly more often than thoracic or infraceliac branches ($p<0.05$, Figure 3d). The celiac, mesenteric and right renal arteries were protected from ostium rupture, while the left suprarenal artery was affected significantly more often than any of the other major side branches ($p<0.05$, Figure 3d). Moreover, all IMHs started and ended near the ostium of a minor or major side branch (Figure 3a, 3e). All thoracic IMHs (n= 10/10) ended at the left subclavian artery, while the cranial end of IMHs that were limited to the abdominal aorta was marked by a supraceliac minor branch (n=12/13) or the left suprarenal artery (n=1/13). The caudal end of the IMHs occurred either at the trifurcation of mesenteric and right renal arteries (n=8/23), the left renal artery (n=7/23) or a minor branch in the thoracic (n=1/23) or infraceliac aorta (n=7/23) (Figure 3e).

PCXTM-based analysis of medial tear and false channel formation at the ostium of the celiac and mesenteric arteries

Since both early-stage Exitron infiltration (Figure 1b) and late-stage medial tear formation (Figure 3c) were most frequent near the celiac and mesenteric arteries, we analyzed the location of medial tears near these branches in detail (Figure 4a). In animals that were found dead or sacrificed after 10, 18 or 28 days of Ang II-infusion, all 25 tears near the ostium of celiac and mesenteric arteries occurred on either the left or the ventral aspect of the aorta, with 0 cases on the dorsal or the right aspects ($p<0.05$, Figure 4a). Interestingly, there was no correlation between the length of the medial tear and the volume of free-flowing blood outside the tunica media (Figure 4b). Rather than the length of the tear, what mattered for the formation of a so-called

false channel was the tear location: medial tears that were located on the left quadrant of the aorta and affected the ostium of both celiac and mesenteric arteries resulted in a significantly larger volume of free-flowing blood outside the media than ventral tears or left tears that were restricted to the ostium of the celiac or the mesenteric artery ($p<0.05$, Figure 4c). Interestingly, the volume of coagulated blood inside the IMH did not increase correspondingly (Figure 4d).

In vivo imaging: dissecting aneurysm evolution over time

BMode ultrasound images show the development of a false channel in the supraceliac region, and Colour Doppler visualized vortex formation inside (Figure 5a). However, in vivo ultrasound-based detection of dissecting aneurysms was strongly dependent on the type of lesion (Figure 5b). At day 3 only 1 dissecting aneurysm was detected in vivo (Figure 1e-i). At day 10 a dissecting aneurysm was detected in vivo in 13/24 surviving animals (2/14 aneurysm ruptures occurred after day 10). These numbers remained constant over time, with 11/19 detections at day 18 and 8/14 at day 28 (Figure 5b). Most non-detected animals belonged to the category without IMH and without false channel (green dots). Follow-up micro-CT allowed for in vivo imaging of the 3D lumen at different time points, and also allowed to visualize infiltrated Exitron from earlier scans at the latest time points (Figure 5c). Once detected, the extra-luminal volume of free-flowing blood increased over time in only n=2/9 animals that were followed up at 2 or more different time-points, both of them with a false channel (Figure 5d).

The overall supraceliac aortic diameter as detected with ultrasound was significantly higher at day 10 than at baseline but remained at the same value after day 10, thus confirming micro-CT volume data (Figure 5e). Interestingly, animals without an IMH had a significantly lower baseline diameter in the supraceliac aorta than animals with an IMH. The difference was not present in the infrarenal aortic diameter (Figure 5f). The supraceliac circumferential strain was already decreased after 3 days and reached a significantly lower value after 10 days to remain constant after that (Figure 5g). There was no difference in supraceliac backflow over time, but the infrarenal aorta experienced a significant increase in diastolic backflow after 10 days of Ang II infusion, which subsequently remained constant over time (Figure 5h).

Image-guided histology: wall remodeling over time

Image-guided histology allowed us to visualize intramural erythrocytes (Figure 6a) and collagen deposition (Figure 6b) at five different time points and in three different aortic locations. Both at the level of the ruptured left suprarenal artery and cranial to the false channel the integrity of intima and media was intact at all three time points, confirming that the source of the bleeding was in a more distal tract (Figure 6a, 6b, top and middle). In the middle of the false channel the medial layered architecture was focally fully lost and the bleeding from the mural rupture caused a focal separation of the abluminal layers of the media. The margins of the dissected vessel were connected to each other by means of a thrombus that penetrated into the adventitia and periaortic adipose tissue (Figure 6a, 6b, bottom).

The amount of intact erythrocytes within the IMH was highest at day 10 (Figure 6c). However, marked differences could be observed between different aortic locations. Just cranial to the false channel the entire intramural space was filled with intact erythrocytes, but at the ruptured ostium of the left suprarenal artery most of the IMH

consisted of fibrin with only a small layer of still intact erythrocytes at the periphery (Figure 6a). In all mice there was a significant increase in medial thickening that started after 10 days of Ang II infusion and staid constant after that ($p<0.05$, Figure 6d). At the latest time point no more percolated red blood cells were visible as they were replaced by spindle cells, collagen deposition and a few haphazardly arranged capillaries (granulation tissue) (Figure 6e). Adventitial remodeling started at the outer edges and strongly depended on the aortic location (Figure 6a, 6b), while adventitial thickening only reached significance from day 18 on (Figure 6f).

Discussion

Connecting the dots: short answers to long-standing questions

In 2015 we published a PCXTM-based study in which we suggested that suprarenal branch ruptures were a potential cause for IMH formation in n=15 Ang II-infused, anti-TGF-Beta treated C57Bl6 mice[9]. Where our earlier work accurately described some cases that we thought representative, the current paper set out to characterize, structure and explain this variability in a large dataset of ApoE $^{-/-}$ mice. We hereby focused on the three open questions that were introduced at the onset of our study:

1. **The suprarenal location of dissecting aneurysms.**

We demonstrated how micro-ruptures occur near the orifice of aortic side branches at an early stage of the disease (Figure 1). These micro-ruptures form in both the thoracic and the abdominal aorta, but occur most frequently near the ostium of 2 specific side branches: the celiac and mesenteric arteries. These observations were also reflected in the location of medial tears in fully developed dissecting aneurysms (Figure 3): thoracic tears sometimes happen near intercostal arteries, but most medial tears are found near the ostium of celiac and mesenteric arteries. We conclude that these aortic branches play a crucial role in the suprarenal location of dissecting aneurysms.

2. **The variability of dissecting aneurysms.**

The categorization of 34 abdominal lesions into 7 different categories allowed us to disentangle the effect of medial tears (which occurred in 31/34 mice), IMHs (which only occurred in 23/31 animals with a medial tear) and false channels (which only occurred in 11/23 animals with an IMH) (Figure 2). Importantly, these categories clearly demonstrate that not all animals that are given angiotensin II will experience luminal dilatation in the form of a large false channel. We subsequently showed that the circumferential location of the medial tear was a more important indicator for false channel formation than tear length (Figure 4). Indeed, animals with a large medial tear that occurred ventral to the celiac or mesenteric ostium did not form a false channel, while right or dorsal tears were not observed at all. We conclude that medial tear location plays a crucial role in the variability of dissecting aneurysms.

3. **The sequence of events in dissecting aneurysm formation**

Based on our remarkably consistent observations on the location of micro-ruptures and medial tears we came up with an elaborate set of hypotheses for what we think is the sequence of events in dissecting aneurysm formation (Figure 7). We propose a six-step mechanism, where different outcomes at each intermediate step affect the final lesion shape and, thus, the observed lesion variability. We propose that each dissecting aneurysm is initiated by a micro-rupture, most often near the celiac or mesenteric artery, which subsequently propagates into a medial tear. In a subset of cases where the aortic diameter at the level of the medial tear is sufficiently large, the tension on the adventitia (which is directly exposed to the blood pressure at the level of the tear) causes the latter to dissect. This adventitial dissection subsequently causes small side branches to rupture, which results in additional inflow of blood into the intramural space and the formation of an IMH. We hypothesize that the propagation of such an adventitial dissection is hampered by the anchoring force of large side branches and propagated by the rupture of small side branches. That is why an adventitial dissection triggered by a medial tear near the celiac artery will

result in an IMH that is larger in the left supraceliac direction (where the small left suprarenal artery cannot withstand the dissection) than in the right infraceliac direction (where the trifurcation of mesenteric and right renal arteries anchors and stabilizes the dissection). If the adventitial dissection is not stopped by any branch, the adventitia ruptures and the animal succumbs to hemothorax or hemoabdomen. In surviving animals, the adventitial dissection is stopped in both cranial and caudal direction by an anchoring side branch (in the thoracic aorta usually the left subclavian artery). Once the dissection has stabilized, the IMH will start to remodel. A false channel will form within the IMH if the medial tear is located within a part of the IMH where the adventitia is dissected far from the media, such that the intramural blood flow is sufficiently strong to prevent coagulation. For IMHs that were triggered by a tear near the celiac artery, this is the case for large medial tears that run on the left side of the aorta – where the IMH is largest and the adventitia is not kept in place by the trifurcation of mesenteric and right renal arteries.

A detailed explanation of these hypotheses and an argumentation for their validity can be found in the online data supplement.

Putting things into perspective: a comparison with literature

At first sight, the data presented in this manuscript seem to contradict a number of publications that have been published on the Ang II-infused mouse model. We believe, however, that rather than creating controversy, our data provide a unique opportunity to put some of the previously published findings into perspective. Already in 2001, Daugherty *et al*. were the first to classify the heterogeneity of Ang II-induced aneurysm morphology into 4 different grades [5]. Sixteen years later, we can re-interpret that *grade I* aneurysms had a medial tear in the abdominal aorta that did not lead to an IMH (n=7/34, green dots in Figure 2a), while *grade IV* aneurysms had a thoracic tear with an IMH that extended all the way down to the suprarenal aorta (n=6/34, cyan and blue dots in Figure 2a). The somewhat artificial difference between the non-descript *grade II* aneurysms and the bulbous-shaped *grade III* aneurysms, on the other hand, makes perfect sense when the so-called `bulbous shape` is re-interpreted as due to the absence (n=9/34, magenta dots in Figure 2a) or presence (n=8/34, red dots in Figure 2a) of a parallel false channel. The existence of Ang II-induced lesions with (i) a thoracic medial tear (n=7/34), (ii) a false channel in the thoracic aorta (n=3/34), or (iii) an IMH that extends into the infrarenal aorta (n=10/34) are usually not reported in literature. At the same time, these findings are not incompatible with any published paper on the model either, for the simple reason that almost all research papers that use Ang II-infused mice focused exclusively on the suprarenal aspect of the aorta in their analysis [2].

In 2003, Saraff *et al* were the first to report that aortic dissection is the dominant mechanism in aneurysm formation of Ang II-infused mice. The authors argued that Ang II-infused mice should nevertheless be considered a good model for human aneurysm formation [21]. But in their seminal paper Saraff *et al* did not discuss the heterogeneity of abdominal lesions as described by Daugherty *et al* [5] and as depicted in Figure 2. Instead, they claimed that all murine AAAs were limited to the suprarenal aorta and that all Ang II-induced lesions followed a similar pattern: a dissection happening between 3 and 10 days after the start of Ang II infusion, subsequently followed by re-endothelialization, luminal dilatation and thrombus remodeling. While

this is certainly true for some of the lesions, our data reveal an underlying reality that is much more complex and much less uniform (in both mechanism and timing).

In 2005, Barisione *et al* showed that dissecting aneurysms experience a continuous increase of luminal diameter throughout the first 28 days of Ang II infusion [22]. In 2011, Rateri *et al* confirmed these findings, reporting a continued expansion of the luminal diameter up to 84 days after the start of Ang II infusion [23]. At first sight these data contradict our in vivo ultrasound and micro-CT data, in which we noticed a stagnation of the aortic diameter after 10 days (Figures 4b and 4f). In this respect it is important to note three things. First of all, our study was set up in order to describe the mechanisms behind aortic variability, not in order to describe the in vivo increase in luminal diameters. As a consequence, 4-5 animals with obvious dissecting aneurysm presence (as detected on ultrasound) were sacrificed at each intermediate imaging time point and the mice in which no obvious luminal dilatation occurred (medial tear but no IMH), were over-represented at later time points (green dots in Figure 5). This phenomenon largely contributed to the apparent stagnation of the supraceliac aortic diameter in Figure 5e. A second argument is that the studies of Barisione *et al* and Rateri *et al* used a Vevo 660 to measure aortic diameters. This older version of the VisualSonics apparatus did not dispose of Color Doppler ultrasound to discriminate between regions with and regions without aortic flow. Without Color Doppler, the large dilated area of the IMH can be misclassified as a dilated lumen (see, for example, the top panel in Figure 5a and images in [24, 25]) and interpreted as an increase of lumen diameter (rather than outer diameter) over time. This is directly related to a third possible explanation for the observed difference: that the continuous increase of aortic lumen diameter in literature is mainly driven by the animals with a false channel. Indeed, when we determined aortic volumes accurately in 3D with contrast-enhanced micro-CT, a technique that only visualizes the aortic lumen and thus by definition avoids any confusion with the IMH [14], we found that the suprarenal diameter increase was much more outspoken in the animals with a false channel than in animals without false channel (Figure 5d). This finding was confirmed when analyzing the 2D ultrasound lumen diameter data per lesion type (Figure 5e). Instead, Rateri *et al* [23], similar to Barisione *et al* [22] and Saraff *et al* [21], reported on luminal dilatation as if it occurred similarly and uniformly in all mice. None of these authors explicitly denied the heterogeneity of the model as described by Daugherty *et al* [5], but neither did they actively discriminate between mice with and mice without false channel in their conclusions.

Citing the +200 papers that have described the Ang II model or used it in treatment studies to enhance or reduce AAA formation would be beyond the scope of this manuscript. It is, however, noteworthy that pharmacological studies published in 2016 still use a 50% luminal diameter increase criterion to define AAA incidence in Ang II infused mice [26]. But if one would really restrict all observations to those with a 50% increase in *luminal* diameter, one would essentially have to restrict the mouse model to the subset of cases in which a suprarenal abdominal tear leads to a false channel (n=8/34 in the current study, which corresponds to the incidence of 29% grade III aneurysms that was reported in a previously published meta-analysis[2]). Rather than quantifying the efficacy of a given treatment through its effect on the maximal luminal diameter, we believe therefore that pharmacological studies should focus on the three criteria that influence the final morphology: medial tear, IMH and false channel. In our opinion some researchers should, however, not only question

the efficacy of their methodology to quantify AAA incidence in these mice, but also whether Ang II-infusion is the appropriate model to answer their research question.

Ang II-infusion into ApoE -/- mice: a model for aortic dissection?

Our results highlight some remarkable differences between dissecting aneurysms and human AAAs, such as the presence of (i) a focal medial tear at specific branch-related regions rather than circumferential medial degradation, (ii) an IMH caused by adventitial dissection rather than an intraluminal thrombus and (iii) a false channel increasing in size in a subset of animals rather than a gradual luminal dilatation in all subjects. On the other hand, we also identified some previously unreported features that might be clinically relevant for human AD, such as the difference between fully occluded IMHs and IMHs with partial thrombosis [15] and the importance of side branches on medial tear location, IMH severity and false channel formation. Based on these observations we conclude that, as long as all limitations of the model are taken into account, Ang II-infused mice might be better suited for future research on aortic dissection than for research on aortic aneurysm.

Limitations and future work

Our study was limited to male ApoE $^{-/-}$ mice of 12 weeks old that received a dose of 1000 ng/mg/kg Ang II and were on a normal diet. In a recent meta-analysis we demonstrated that sex, genetic background, age, and low dose significantly influence dissecting aneurysm incidence while high dose and high fat diet do not [2]. The goal of the current manuscript, however, was not to understand why some risk factors have more effect than others, but rather to understand what happens with these animals once the initial lesion has occurred. For this purpose we strived for uniformity, rather than diversity, in the confounding factors to which our mice were exposed.

Since we used fixed time points it was not possible to know how long each lesion had been in place at the moment of sacrifice, which was reflected in the relatively large inter-subject variability of histology results (Figure 6). In general, the fact that sample sizes were not sufficiently large to compare different dissecting aneurysm categories at each time point is a limitation of our study. It is, however, important to point out that the variability in histology was not only due to differences in time or dissecting aneurysm category. The amount of collagen and erythrocytes also varied greatly within the same animal and depended (amongst others) on the distance from the medial tear and on the local dimensions of the IMH. This important finding confirms previous reports [6] and should be kept in mind when analyzing stains from dissecting IMHs in which the location of the medial tear is unknown. It is also the reason why all major conclusions of this manuscript have been based on the 3D information that was available from PCXTM scans.

In future work we aim to deepen our understanding of dissecting aneurysms and, as long as the implications are not over-interpreted, their implications for human AD and AAA. Finite element simulations of the biomechanics after only few days of Ang II infusion will hopefully provide more insight into the reasons why micro-ruptures and medial tears occur so often in the vicinity of celiac and mesenteric arteries, and allow us to compare the influence of local stress concentrations near these branches to other potential explanations such as local differences in expression of Ang II receptors, hemodynamics[17], soft tissue mechanics[27] or leftward curvature and

leftward pulsatility of the aorta[28]. Similarly, modelling the mechanobiology at the interface between false channel and IMH will allow us to better understand how, once the false channel has formed, the interplay between free flowing blood and IMH affects the stability of the lesions[15].

Funding

This research was funded by the Special Research Fund of Ghent University and by internal funds of the Laboratory of Hemodynamics and Cardiovascular Technology, EPFL. Bram Trachet is supported by a research grant of the Research Fund Flanders (FWO, grant 12A5816N).

Acknowledgments

The authors would like to thank Dr. Alberto Astolfo, Dr. Orestis Vardoulis, Dr. Carole Van der Donckt and Bieke Vanderveken for their assistance during the PCXTM scans. Further we wish to acknowledge Agnès Hautier and the entire team of the Histology Core Facility at the Ecole Polytechnique Fédérale de Lausanne (EPFL) for their technical expertise with the PCXTM-guided histology, Dr. José Artacho from the Bioimaging and Optics platform (PTBIOP) at EPFL for his expert help with the image data processing and Fotis Savvopoulos for his help processing the in vivo ultrasound data. We also thank Marion Varet, Celine Waldvogel and the entire team of the Phenotyping Unit in the Center of PhenoGenomics at the school of Life Sciences in EPFL for their technical and scientific expertise in the micro-CT experiments, as well as Dr. Mauro Ferraro for his feedback on the project and the manuscript.

Conflict of interest

None.

References

1. Daugherty A, Rateri DL, Charo IF, Owens AP, Howatt DA, Cassis LA. Angiotensin II infusion promotes ascending aortic aneurysms: attenuation by CCR2 deficiency in apoE-/- mice. *Clinical science (London, England : 1979)* 2010;**118**:681-689.
2. Trachet B, Fraga-Silva RA, Jacquet P, Stergiopulos N, Segers P. Incidence, mortality and confounding factors for AAA detection in angiotensin II-infused mice: a meta-analysis. *Cardiovasc Res* 2015;**108**:159-170.
3. Daugherty A, Manning MW, Cassis LA. Angiotensin II promotes atherosclerotic lesions and aneurysms in apolipoprotein E-deficient mice. *J Clin Invest* 2000;**105**:1605-1612.
4. Senemaud J, Caligiuri G, Etienne H, Delbosc S, Michel J-B, Coscas R. Translational Relevance and Recent Advances of Animal Models of Abdominal Aortic Aneurysm. *Arterioscler Thromb Va− c Biol* 2017.
5. Daugherty A, Manning MW, Cassis LA. Antagonism of AT2 receptors augments Angiotensin II-induced abdominal aortic aneurysms and atherosclerosis. *Br J Pharmacol* 2001;**134**:865-870.
6. Schriefl AJ, Collins MJ, Pierce DM, Holzapfel GA, Niklason LE, Humphrey JD. Remodeling of Intramural Thrombus and Collagen in an Ang-II Infusion ApoE−/− Model of Dissecting Aortic Aneurysms. *Thromb Res* 2012;**130**:e139-e146.
7. Gavish L, Beeri R, Gilon D, Rubinstein C, Berlatzky Y, Gavish LY, Bulut A, Harlev M, Reissman P, Gertz SD. Inadequate reinforcement of transmedial disruptions at branch points subtends aortic aneurysm formation in apolipoprotein-E-deficient mice. *Cardiovasc Pathol* 2014;**23**:152-159.
8. Raffort J, Lareyre F, Clement M, Hassen-Khodja R, Chinetti G, Mallat Z. Monocytes and macrophages in abdominal aortic aneurysm. *Nat Rev Cardiol* 2017;**advance online publication**.
9. Trachet B, Fraga-Silva RA, Piersigilli A, Tedgui A, Sordet-Dessimoz J, Astolfo A, Van der Donckt C, Modregger P, Stampanoni M, Segers P, Stergiopulos N. Dissecting abdominal aortic aneurysm in ang II-infused mice: suprarenal branch ruptures and apparent luminal dilatation. *Cardiovasc Res* 2015;**105**:213-222.
10. Xanthoulea S, Thelen M, Pöttgens C, Gijbels MJJ, Lutgens E, de Winther MPJ. Absence of p55 TNF Receptor Reduces Atherosclerosis, but Has No Major Effect on Angiotensin II Induced Aneurysms in LDL Receptor Deficient Mice. *PLoS ONE* 2009;**4**:e6113.
11. Trachet B, Fraga-Silva RA, Piersigilli A, Segers P, Stergiopulos N. Dissecting abdominal aortic aneurysm in ang II-infused mice: the importance of imaging. *Curr Pharm Des* 2015;**21**:4049-4060.
12. Hiratzka LF, Bakris GL, Beckman JA, Bersin RM, Carr VF, Casey DE, Eagle KA, Hermann LK, Isselbacher EM, Kazerooni EA, Kouchoukos NT, Lytle BW, Milewicz DM, Reich DL, Sen S, Shinn JA, Svensson LG, Williams DM. 2010 ACCF/AHA/AATS/ACR/ASA/SCA/SCAI/SIR/STS/SVM Guidelines for the Diagnosis and Management of Patients With Thoracic Aortic Disease. *A Report of the American College of Cardiology Foundation/American Heart Association Task Force on Practice Guidelines, American Association for Thoracic Surgery, American College of Radiology, American Stroke Association, Society of Cardiovascular Anesthesiologists, Society for Cardiovascular Angiography and Interventions, Society*

656 *of Interventional Radiology, Society of Thoracic Surgeons, and Society for Vascular*
657 *Medicine* 2010;**121**:e266-e369.
658 13. Humphrey JD, Schwartz MA, Tellides G, Milewicz DM. Role of
659 Mechanotransduction in Vascular Biology: Focus on Thoracic Aortic Aneurysms and
660 Dissections. *Circ Res* 2015;**116**:1448-1461.
661 14. Trachet B, Fraga-Silva RA, Londono FJ, Swillens A, Stergiopulos N, Segers P.
662 Performance Comparison of Ultrasound-Based Methods to Assess Aortic Diameter
663 and Stiffness in Normal and Aneurysmal Mice. *PLoS ONE* 2015;**10**:e0129007.
664 15. Tsai TT, Evangelista A, Nienaber CA, Myrmel T, Meinhardt G, Cooper JV, Smith
665 DE, Suzuki T, Fattori R, Llovet A, Froehlich J, Hutchison S, Distante A, Sundt T,
666 Beckman J, Januzzi JLJ, Isselbacher EM, Eagle KA. Partial Thrombosis of the
667 False Lumen in Patients with Acute Type B Aortic Dissection. *N Engl J Med*
668 2007;**357**:349-359.
669 16. Corvera JS. Acute aortic syndrome. *Annals of Cardiothoracic Surgery* 2016;**5**:188-
670 193.
671 17. Trachet B, Renard M, De Santis G, Staelens S, De Backer J, Antiga L, Loeys B,
672 Segers P. An integrated framework to quantitatively link mouse-specific
673 hemodynamics to aneurysm formation in angiotensin II-infused ApoE -/- mice. *Ann*
674 *Biomed Eng* 2011;**39**:2430-2444.
675 18. Wang Y, Ait-Oufella H, Herbin O, Bonnin P, Ramkhelawon B, Taleb S, Huang J,
676 Offenstadt G, Combadiere C, Renia L, Johnson JL, Tharaux P-L, Tedgui A, Mallat Z.
677 TGF-beta activity protects against inflammatory aortic aneurysm progression and
678 complications in angiotensin II-infused mice. *J Clin Invest* 2010;**120**:422-432.
679 19. Schindelin J, Arganda-Carreras I, Frise E, Kaynig V, Longair M, Pietzsch T, Preibisch
680 S, Rueden C, Saalfeld S, Schmid B, Tinevez J-Y, White DJ, Hartenstein V, Eliceiri K,
681 Tomancak P, Cardona A. Fiji - an Open Source platform for biological image analysis.
682 *Nat Methods* 2012;**9**:10.1038/nmeth.2019.
683 20. Trachet B, Piersigilli A, Fraga-Silva RA, Aslanidou L, Astolfo A, Stampanoni MFM,
684 Segers P, Stergiopulos N. Ascending aortic aneurysm in angiotensin II infused mice:
685 Formation, progression and the role of focal dissections. *Arterioscler Thromb Va−c*
686 *Biol* 2015;**36**:673-681.
687 21. Saraff K, Babamusta F, Cassis LA, Daugherty A. Aortic dissection precedes formation
688 of aneurysms and atherosclerosis in angiotensin II-infused, apolipoprotein E-deficient
689 mice. *Arterioscler Thromb Va−c Biol* 2003;**23**:1621-1626.
690 22. Barisione C, Charnigo R, Howatt DA, Moorleghen JJ, Rateri DL, Daugherty A. Rapid
691 dilation of the abdominal aorta during infusion of angiotensin II detected by
692 noninvasive high-frequency ultrasonography. *J Vasc Surg* 2006;**44**:372-376.
693 23. Rateri DL, Howatt DA, Moorleghen JJ, Charnigo R, Cassis LA, Daugherty A.
694 Prolonged Infusion of Angiotensin II in apoE−/− Mice Promotes Macrophage
695 Recruitment with Continued Expansion of Abdominal Aortic Aneurysm. *Am J Pathol*
696 2011;**179**:1542-1548.
697 24. Cao RY, Amand T, Ford MD, Piomelli U, Funk CD. The Murine Angiotensin II-
698 Induced Abdominal Aortic Aneurysm Model: Rupture Risk and Inflammatory
699 Progression Patterns. *Front Pharmacol* 2010;**1**:9-9.
700 25. Sampson UK, Perati PR, Prins PA, Pham W, Liu Z, Harrell FE, Jr., Linton MF, Gore
701 JC, Kon V, Fazio S. Quantitative Estimates of the Variability of In Vivo Sonographic
702 Measurements of the Mouse Aorta for Studies of Abdominal Aortic Aneurysms and
703 Related Arterial Diseases. *J Ultrasound Med* 2011;**30**:773-784.

26. Alsiraj Y, Thatcher SE, Charnigo R, Kuey C, Blalock E, Daugherty A, Cassis LA. Female Mice with an XY Sex Chromosome Complement Develop Severe Angiotensin II-Induced Abdominal Aortic Aneurysms. *Circulation* 2016.
27. Trachet B, Bols J, Degroote J, Verhegghe B, Stergiopulos N, Vierendeels J, Segers P. An animal-specific FSI model of the abdominal aorta in anesthetized mice *Ann Biomed Eng* 2015;**43**:1298-1309.
28. Goergen CJ, Azuma J, Barr KN, Magdefessel L, Kallop DY, Gogineni A, Grewall A, Weimer RM, Connolly AJ, Dalman RL, Taylor CA, Tsao PS, Greve JM. Influences of Aortic Motion and Curvature on Vessel Expansion in Murine Experimental Aneurysms. *Arteriosclerosis Thrombosis and Vascular Biology* 2011;**31**:270-U102.

Figure legends

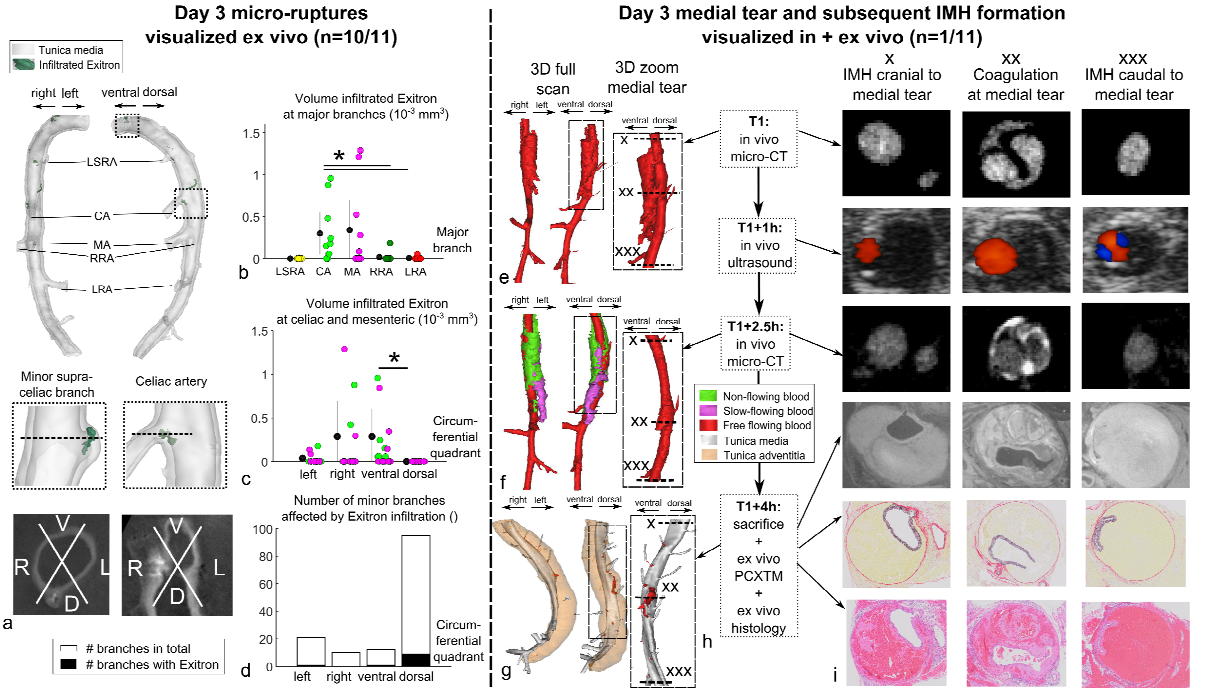

Figure 1. Early events in Angiotensin II-infused mice. a. 3D (segmented) and 2D PCXTM images of early-stage damage as visualized with Exitron. **b.** Scatter plot showing the volume of Exitron infiltration at each of the 5 major branches. **c.** Scatter plot showing how the volume of Exitron infiltration varies across the circumference of celiac and mesenteric arteries (quadrants as in panel a, bottom right). **d.** Bar plot showing how the number of minor branches affected by Exitron infiltration varies across the circumference (quadrants as in panel a, bottom left). **e-g.** 3D (segmented) micro-CT (top, middle) and PCXTM (bottom) showing how the free-flowing blood outside the media and the resulting IMH evolved over time in the case of a live rupture. **h.** Timeline of in and ex vivo scans performed on the case of live rupture. **i.** 2D slices visualizing how free-flowing blood coagulated into an IMH within few hours. Top-bottom: micro-CT shows a false channel at T1, Color Doppler ultrasound shows absence of blood flow in the IMH at T1+1h, micro-CT shows how the false channel is coagulating at T1+2.5h, PCXTM shows coagulation patterns around the tear at T1+4h, SR-Miller stains and HE stains show how coagulation takes places at the tear but not yet at cranial and caudal ends of the IMH at T1+4h. *: $p<0.05$. V: ventral, D: dorsal, R: right, L: left, LSRA: left suprarenal artery, CA: celiac artery, MA: mesenteric artery, RRA: right renal artery, LRA: left renal artery.

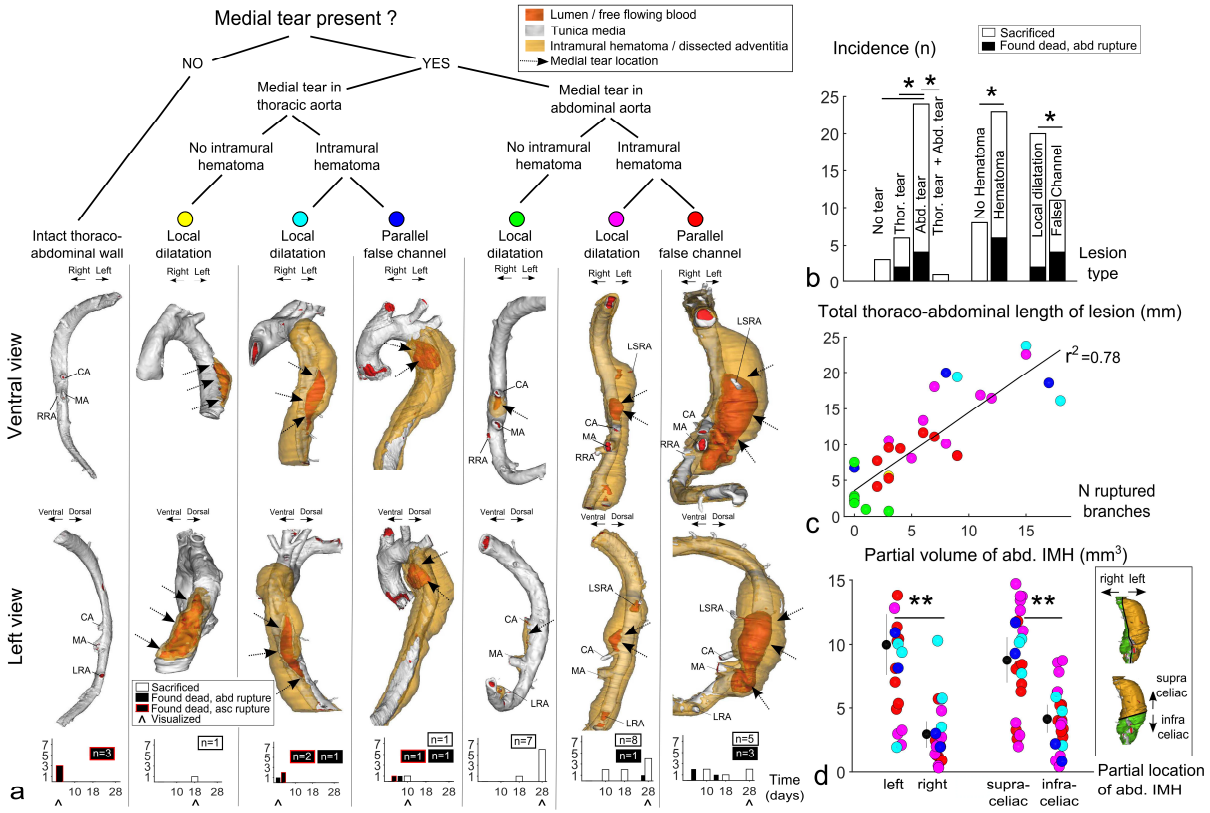

Figure 2. Variability in dissecting aneurysm shape. **a.** Flow chart depicting the different categories of dissecting aneurysms in animals that were found dead or sacrificed after more than 3 days of Ang II infusion (top) and bar plots indicating the cause of death at each time point (bottom). For each category the visualized animal is indicated with ^. **b.** Bar plots showing the dissecting aneurysm incidence (white bars, p-values) and dissecting aneurysm-related mortality (black bars). **c.** Scatter plot showing the correlation between the axial length of the dissecting aneurysm and the number of ruptured side branch ostia. **d.** Scatter plot showing that the volume of the IMH is larger on the left and supraceliac aspects of the aorta. In panels c and d each dot represents one animal, and is colored according to the dissecting aneurysm lesion type as determined by the flowchart in panel a. *: p<0.05. LSRA: left suprarenal artery, CA: celiac artery, MA: mesenteric artery, RRA: right renal artery, LRA: left renal artery.

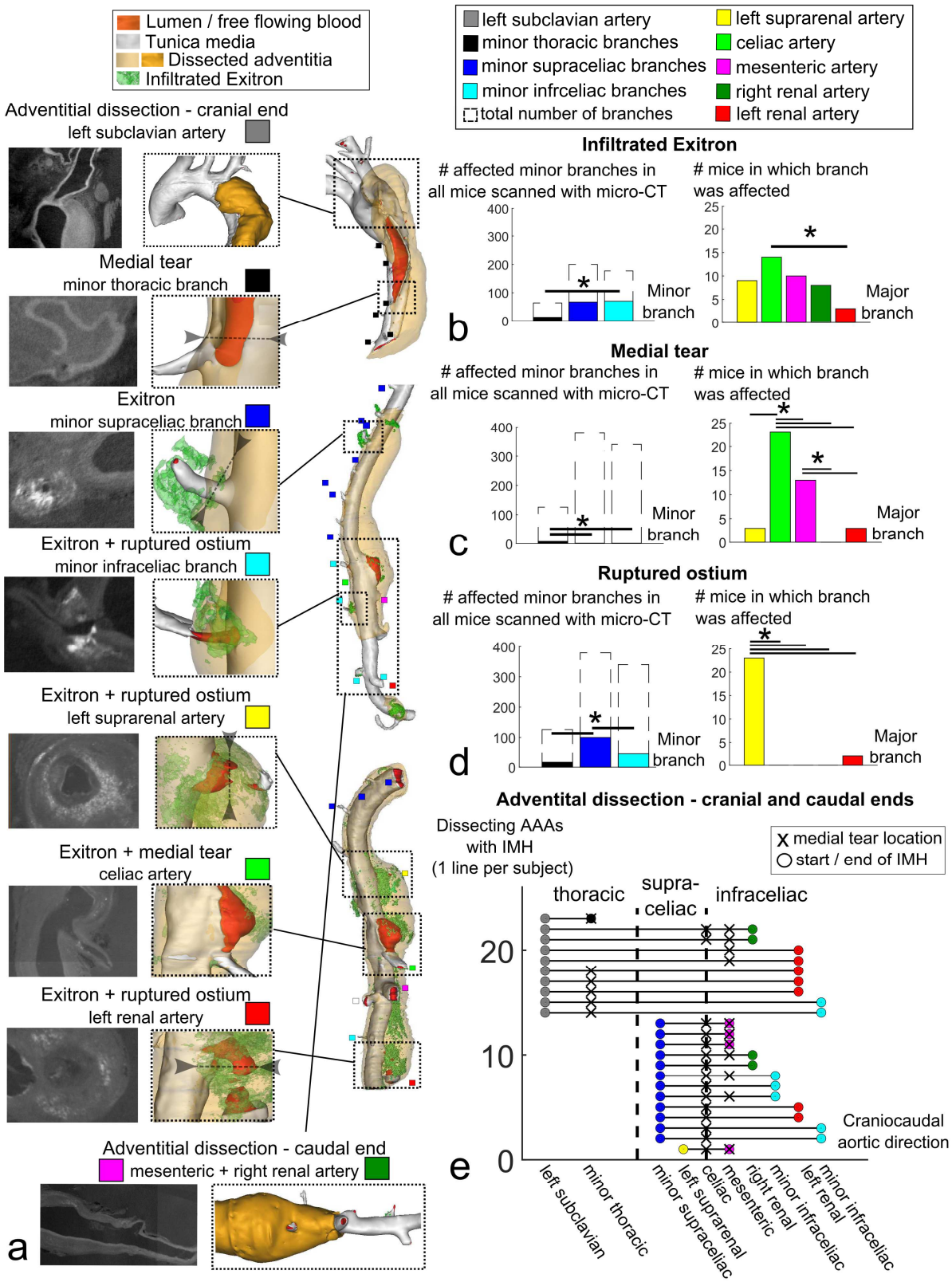

Figure 3. Medial damage near aortic side branches. **a.** 2D and 3D (segmented) PCXTM images of dissecting aneurysms in animals that were found dead or sacrificed after more than 3 days of Ang II infusion. Panels **b-d** indicate the incidence and distribution of Exitron infiltration (**b**), medial tears (**c**) and ruptured ostia (**d**) over major side branches (right panels) and minor side branches (left panels). Each branch is given a color code according to the legend (top). For minor branches the

number of affected branches across all mice was reported, while for major branches we report the number of mice in which each branch was affected. Panel (**e)** schematically shows at which branches the adventitial dissection was stopped (both in cranial and caudal direction) if an IMH was present. Each horizontal line represents a dissected adventitia, each cross represents the location of the medial tear and each endpoint refers to a minor or major branch (colored according to the legend on top). *: $p<0.05$, LSRA: left suprarenal artery, CA: celiac artery, MA: mesenteric artery, RRA: right renal artery, LRA: left renal artery.

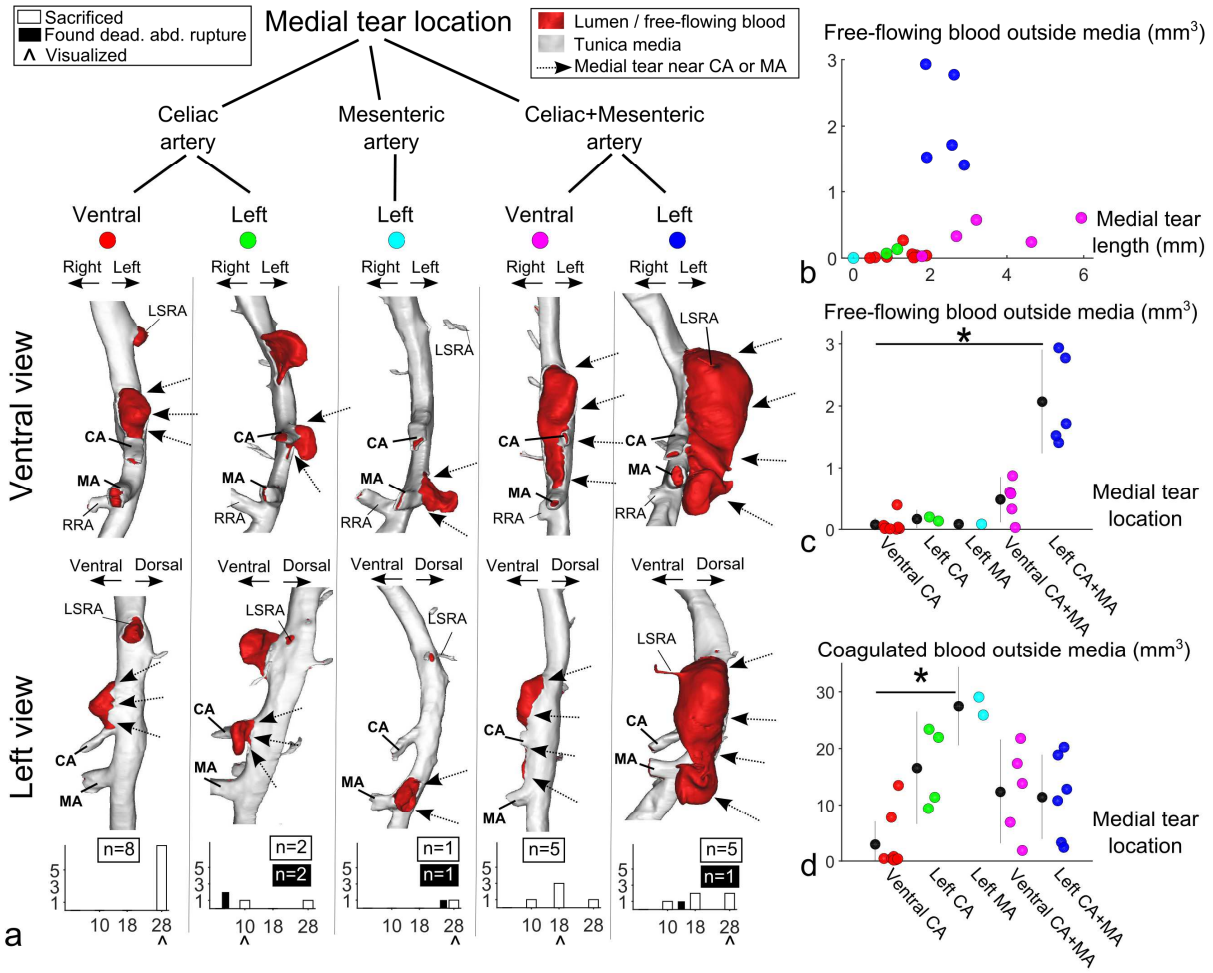

Figure 4. Medial tear location and false channel formation near celiac and mesenteric artery. **a.** Flow chart depicting the different locations at which medial tears were observed near the celiac or mesenteric artery of animals that were found dead or sacrificed after more than 3 days of Ang II infusion (top). Medial tears were defined as a discontinuity of the tunica media on PCXTM images, across all laminae, that was not confined to the ostium of a side branch. Bar plots indicate the cause of death at each time point (bottom), and the visualized animal is indicated with ^. In the 3D segmented PCXTM images the IMH and/or dissecting adventitia have been digitally removed. **b.** Scatter plot showing the (lack of) correlation between the axial length of the medial tear and the volume of free-flowing blood outside the true lumen of the dissecting aneurysm. **c**. Scatter plot showing the influence of tear location on the volume of free-flowing blood outside the tunica media. Notice that a left tear affecting both mesenteric and celiac arteries always results in a false channel. **d.** Scatter plot showing the influence of tear location on the volume of coagulated blood outside the tunica media (i.e. IMH volume). In panels b and c mice that that were found dead were excluded from the analysis since the volume of free-flowing blood could not be determined unambiguously in these cases. In panels b, c and d each dot represents one mouse and is colored according to the location of the medial tear, as determined by the flowchart in panel a. *: $p<0.05$, LSRA: left suprarenal artery, CA: celiac artery, MA: mesenteric artery, RRA: right renal artery, LRA: left renal artery.

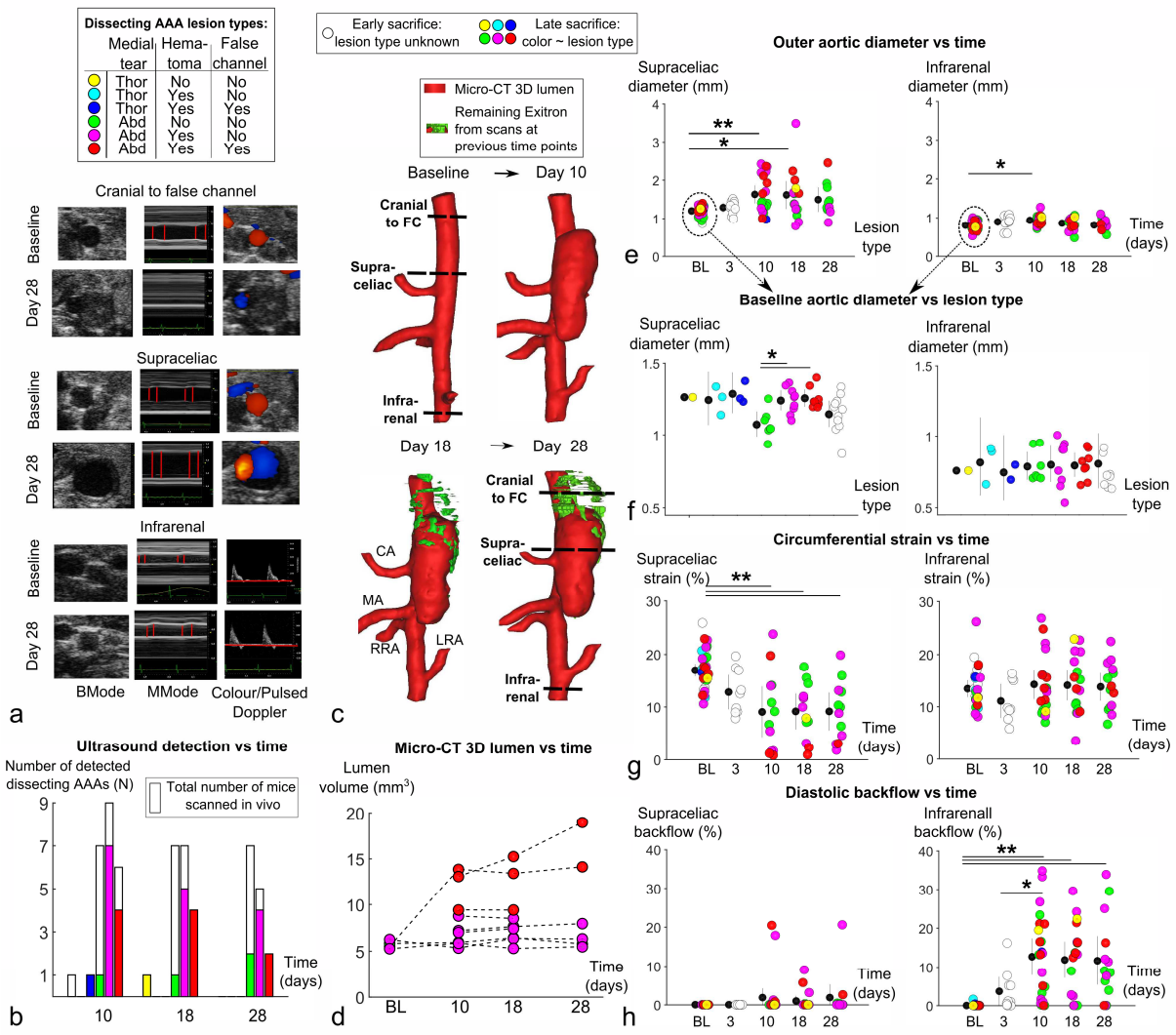

Figure 5. Temporal evolution: in vivo imaging. **a.** 3D segmented micro-CT scans in the same animal at 4 different time points. **b.** Quantification of the volume of free-flowing blood outside the tunica media, based on in vivo micro-CT measurements in the same animals at baseline (volume values overlapping) and subsequent time points (volume values variable). **c.** 2D ultrasound images obtained at the locations indicated in panel c, at baseline and after 28 days of Ang II infusion (in the same animal). BMode, MMode, Colour Doppler: short axis, Pulsed Doppler: long axis. **d.** Bar plot showing the incidence of ultrasound-based in vivo detection of dissecting aneurysms. Detected cases are colored according to their lesion type (see legend on top). The evolution vs time of outer diameter (**e**), circumferential strain (**g**) and diastolic backflow (**h**) is quantified at the supraceliac (left) and the infrarenal (right) aorta. Baseline aortic diameter is shown for different dissecting aneurysm lesion types in panel **f.** Note that the baseline supraceliac diameter was significantly lower in mice that did not develop an IMH afterwards. In panels e-h each dot represents one mouse and was colored according to the dissecting aneurysm lesion type (cfr. legend and Figure 2). *: p<0.05, ** p<0.001. BL: baseline.

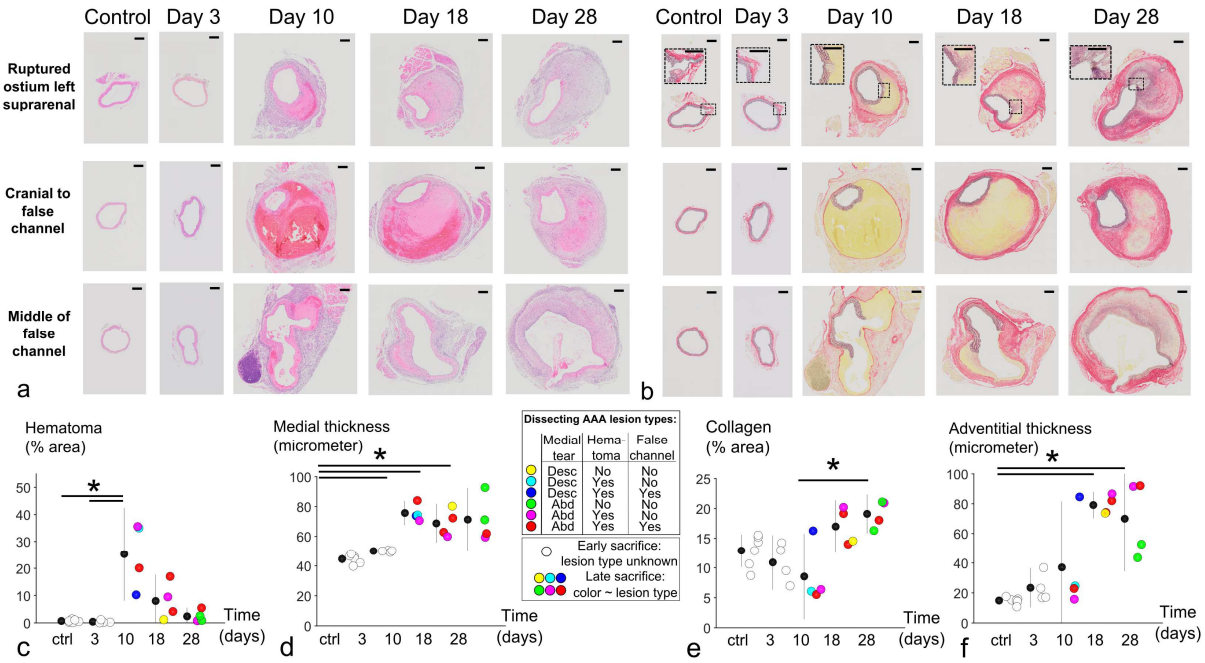

Figure 6. IMH remodeling over time: image-guided histology. For each of 3 aortic locations image-guided stains were obtained from 22 different animals (6 controls and 4 mice at every time point). The stains in panels **a** (H&E: fresh erythrocytes in red, fibrin in pink) and **b** (Sirius Red-Miller: collagen in red, elastin in brown, erythrocytes in yellow) represent different remodeling stages. The scatter plots below quantify the evolution of relative hematoma area (**c**), medial thickness (**d**), relative collagen area (**e**) and adventitial thickness (**f**) over time. In these plots each dot represents a single animal: its value is an average of at least two different stains. Measurements were colored according to the dissecting aneurysm lesion type (cfr. legend and Figure 2). *: $p<0.05$.

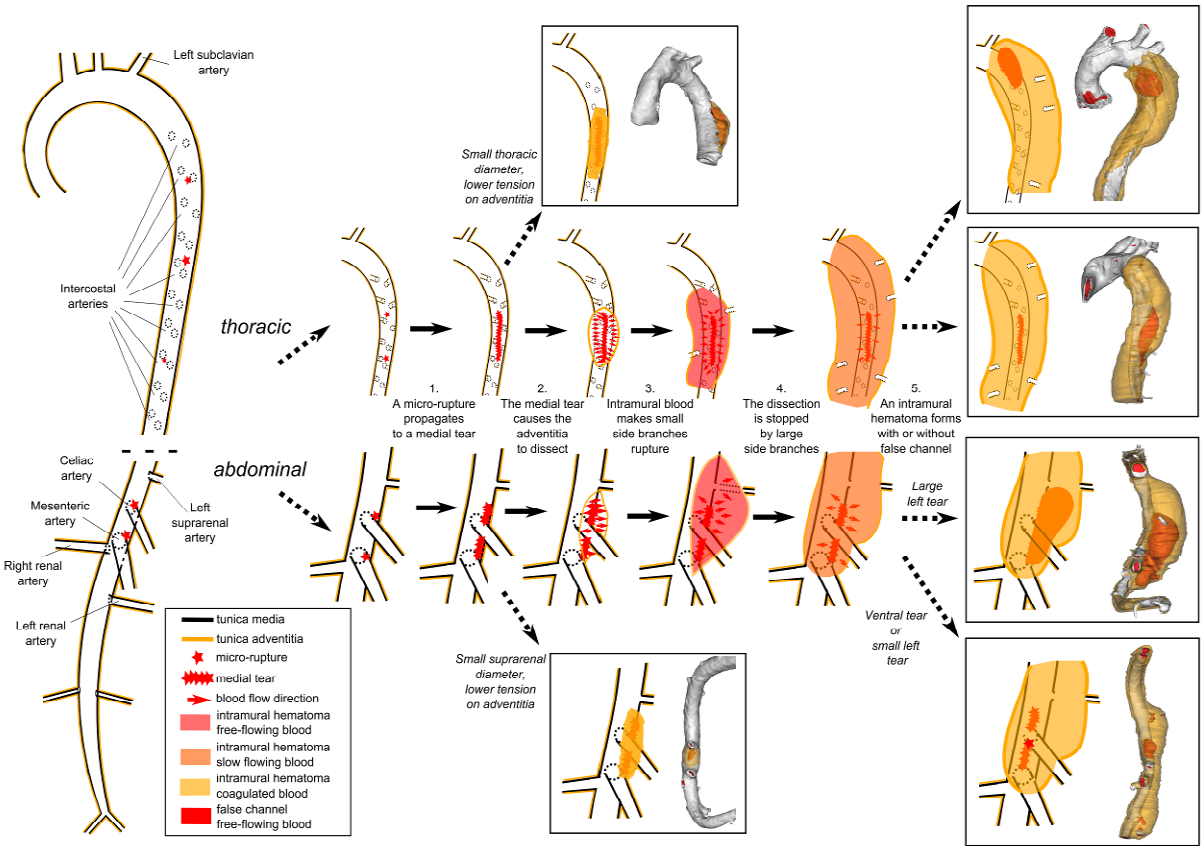

Figure 7. The sequence of events in dissecting aneurysm formation. A schematic representation to illustrate the crucial role of side branches in the initiation and formation of dissecting aneurysms. The mouse aorta with its major branches is depicted on the left. The five different steps in the middle show how micro-ruptures evolve to medial tears and eventually lead to an adventitial dissection and the formation of an IMH with or without false channel. The 6 boxes at the outer edges represent the variability in lesion shapes, which correspond to the experimental results. The reader is referred to Figure 2 for the incidence and mortality rates of each lesion type. Note: this schematic is not to scale and is only intended as an indicative illustration of the five-step hypothesis that is proposed briefly in the manuscript and elaborated on with more details in the online data supplement.